Journal of Sustainable Metallurgy (2020) 6:227–238
https://doi.org/10.1007/s40831-020-00268-5

RESEARCH ARTICLE

On the Direct Reduction Phenomena of Bauxite Ore Using H_2 Gas in a Fixed Bed Reactor

Adamantia Lazou[1] · Casper van der Eijk[2] · Efthymios Balomenos[3] · Leiv Kolbeinsen[1] · Jafar Safarian[1]

Published online: 28 March 2020

Abstract

The Bayer Process is the dominant industrial method to produce alumina from bauxite ore. Due to the generation of large amounts of Bauxite Residue (red mud), an alternative method, called the Pedersen Process, is of our interest. This process makes use of a combination of pyrometallurgical and hydrometallurgical techniques in order to prevent the Bauxite Residue generation. In the conventional Pedersen Process, iron in the bauxite is separated in the form of pig iron through a carbothermic smelting-reduction step which has a CO_2 emission similar to that during conventional iron production. In order to eliminate the CO_2 emission of this step, the focus of the present work is to reduce the iron oxides of bauxite ore by hydrogen gas (H_2) prior to smelting and minimizing the use of solid carbon materials for the reduction. The thermochemistry and the kinetics of reactions during calcination and direct reduction of a bauxite ore were studied by a thermogravimetric technique and in situ analysis of the gaseous products. The onset temperatures for the decomposition of bauxite components during calcination were determined. The kinetics of the reduction of hematite to metallic iron was studied and it is shown that the reduction of iron oxides to metallic iron starts at temperatures below 560 °C and it accelerates at higher temperatures. Moreover, it is indicated that the formation of hercynite ($FeAl_2O_4$) phase retards the complete reduction at temperatures higher than 760 °C.

Keywords Alumina · Bauxite ore · Reduction with hydrogen · Pedersen process

Introduction

Bauxite ore is the main raw material used to produce alumina (Al_2O_3) which is the feedstock for aluminum production. There are three main structural types of aluminum hydroxide minerals in bauxite: gibbsite (γ-$AlO(OH)_3$), boehmite (γ-AlO(OH)), and diaspore (α-AlO(OH)) [1, 2]. Apart from the aluminum minerals, basic components of bauxite also include minerals containing iron, silicon, titanium, calcium, and magnesium [3, 4].

The production of alumina from bauxite occurs mainly through the well-known Bayer Process which is accompanied with the formation of a by-product known as Bauxite Residue (BR). The handling of this residue is a major challenge for the alumina industry and society, mainly due to its high volume and high alkalinity. Depending on the ore characteristics, each metric ton of alumina production causes 1 to 1.5 metric tons of BR production [5]. Many researchers have attempted to find an efficient way to utilize the BR, as it may be a secondary source of metals such as Fe, Ti, Al, and REEs [5]. However, the utilization of BR is still unsolved mostly due to economic reasons. Hence, it is important to find alternative technologies to overcome the environmental problems.

A different approach for alumina production that will prevent BR generation is of interest, and this led us to the Pedersen Process, which had been commercialized in Norway for 40 years before it was closed in 1969 [6]. At that time, the current environmental challenges were not considered important. In the original Pedersen Process as shown in Fig. 1, bauxite was smelted with lime as a flux and coke as the reducing agent. The smelting of bauxite yields pig

The contributing editor for this article was Sharif Jahanshahi.

✉ Adamantia Lazou
Adamantia.Lazou@ntnu.no

[1] Department of Materials Science and Engineering Trondheim, Norwegian University of Science and Technology, NTNU, Trondheim, Norway

[2] SINTEF Materials and Chemistry, Trondheim, Norway

[3] Laboratory of Metallurgy, National Technical University of Athens, NTUA, Athens, Greece

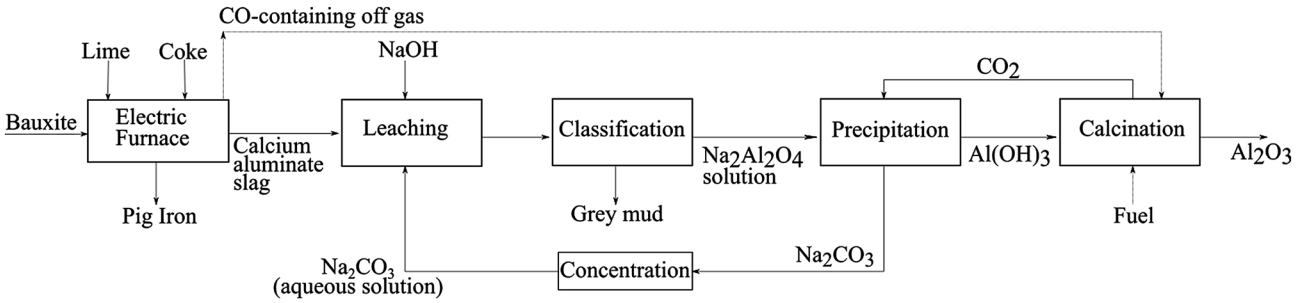

Fig. 1 A schematic of the Pedersen Process for alumina extraction

iron due to the carbothermic reduction of the iron oxides to metallic iron. Furthermore, it yields a calcium-aluminate slag, which is further treated hydrometallurgically for alumina extraction [2, 7, 8].

Significant research efforts on the Pedersen Process at NTNU [9, 10] recently have basis in earlier unpublished work. The results and conditions are sufficiently promising to revive it in a modernized form considering the importance of sustainable approaches in the metallurgical industries. It is worth mentioning that according to our other study [6] it is possible that BR at least partly may serve as a feed stock for this process.

The present work is related to the development of a more sustainable smelting-reduction step where hydrogen replaces metallurgical coke as reducing agent by introduction of a two-stage gaseous pretreatment of the bauxite ore prior to smelting in the electric furnace (EAF). After pre-heating and calcination in the first stage followed by hydrogen reduction in the second stage, the intention is that most of the iron present in the ore charged to the EAF in metallic form.

The main aim of the experiments reported here is to provide a basis for design of a pilot-scale bauxite pretreatment equipment and is generally performed as heating ore samples at a constant rate in inert gas until the intended subsequent reduction temperature (the target temperature) is reached. The gas is then switched to hydrogen for reduction of iron compounds to render most of the iron in metallic state.

The main basis needed for the mentioned equipment design is the chemical analysis and XRD patterns of the samples obtained after the treatment at different target temperatures. However, it is also of interest to try to understand and explain the reactions and processes leading to such observations even if the experimental work is not designed to facilitate such analysis.

Direct Reduced Iron (DRI) production processes [11] have been developed on basis of geographical factors as availability of natural gas; however, they also meet the requirement to reduce greenhouse gas emission and energy consumption. In these processes, there is no need for coke addition and the use of gaseous reductants is more environmentally friendly and less capital demanding than the conventional steel production routes with ironmaking in blast furnaces [12]. In the direct reduction processes, the most common reactor is a shaft furnace and the reduction reactions occur in different stages [12]. The reduction process is usually carried out at temperatures above 570 °C [12] and the different steps of reduction from hematite to metallic iron by hydrogen can be described by the following reactions, (1)–(4), [13, 14]:

$$3\,Fe_2O_3 + H_2 \rightarrow 2\,Fe_3O_4 + H_2O \quad \Delta H_{700\,^\circ C} = 5279\ \text{kJ} \tag{1}$$

$$Fe_3O_4 + 4\,H_2 \rightarrow 3\,Fe + 4\,H_2O \quad \Delta H_{700\,^\circ C} = 95,551\ \text{kJ} \tag{2}$$

$$Fe_3O_4 + H_2 \rightarrow 3\,FeO + H_2O \quad \Delta H_{700\,^\circ C} = 52,086\ \text{kJ} \tag{3}$$

$$FeO + H_2 \rightarrow Fe + H_2O \quad \Delta H_{700\,^\circ C} = 14,488\ \text{kJ}\,. \tag{4}$$

The main objective of the present work was to reduce the iron oxides in bauxite to metallic iron with hydrogen gas (H_2). However, before the reduction of bauxite with H_2 gas, the decomposition of hydroxide minerals and carbonates such as diaspore, goethite, and calcite take place during heating of the ore to the target temperatures, as shown in Eqs. (5)–(7).

$$2(AlO(OH)) = Al_2O_3 + H_2O_{(g)} \tag{5}$$

$$2(FeO(OH)) = Fe_2O_3 + H_2O_{(g)} \tag{6}$$

$$CaCO_3 = CaO + CO_{2(g)}. \tag{7}$$

In Fig. 2, the changes of the Gibbs energy with increasing temperature for chemical reactions (5) and (6) as calculated by HSC Chemistry are shown. Diaspore, AlO(OH) or $Al_2O_3 \times H_2O$, is theoretically decomposed at temperature higher than 300 °C, under 1 atm H_2O vapor pressure,

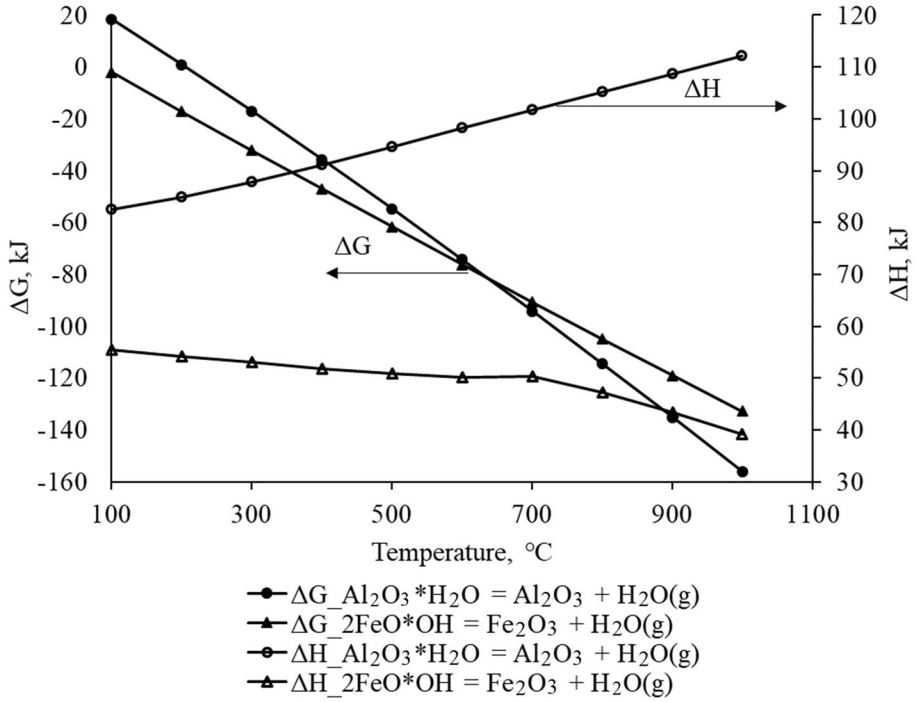

Fig. 2 Standard Gibbs energy and reaction enthalpy changes for the decomposition of diaspore and goethite, calculated by HSC Chemistry (version 9.0)

Table 1 XRF analysis from bauxite ore (wt%)

Oxides	Al_2O_3	Fe_2O_3	CaO	SiO_2	TiO_2	Cr_2O_3	ZrO_2	SO_3	P_2O_5	K_2O	NiO	MgO	LOI
Wt%	62.02	17.01	1.80	2.30	2.50	0.15	0.07	0.06	0.04	0.04	0.02	0.01	13.48

while goethite, FeO(OH), at temperatures higher than 80 °C.

Experimental Procedure

Materials and Characterization

Bauxite ore was provided from Mytilineos S.A, Metallurgy Business Unit (former Aluminium of Greece) as the starting raw material. The ore was crushed to a particle size 5–25 mm and then dried at 105 °C for 24 h. The chemical composition of the ore was determined by X-ray Fluorescence (XRF) and the phase composition characterized by X-ray diffraction (XRD) using Bruker D8 Focus with Cu-Kα radiation, 10° to 75° diffraction angle, 0.02 step size, and 40 kV power.

Bauxite Characteristics

The result of XRF analysis for the ore is presented in Table 1, which shows that the raw bauxite ore has slightly over 60% aluminum oxide and 17% Fe_2O_3. The XRD analysis of the utilized bauxite ore (Fig. 3) shows that the main

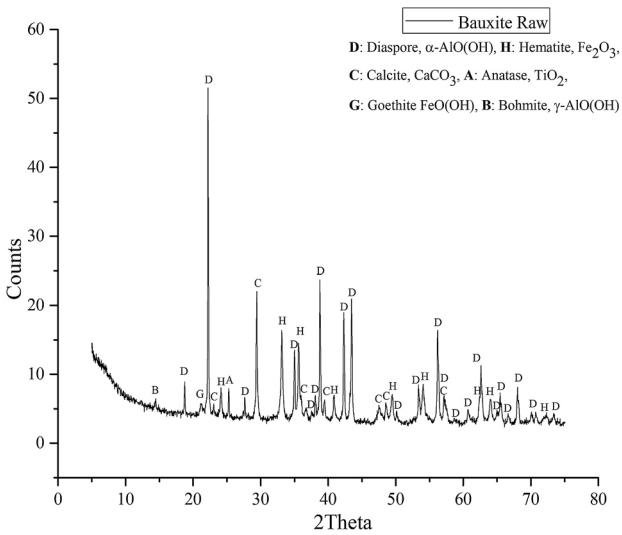

Fig. 3 XRD analysis of bauxite ore and identified phases

Al_2O_3-containing phase is mostly diaspore (α-AlO(OH)) while much less amount of boehmite (γ-AlO(OH)) is detected with the main peak at $2\theta = 14.42°$ [15]. Iron is mainly present as hematite (Fe_2O_3) and a small portion of

goethite (FeO(OH)) with a detected peak at approximately $2\theta = 21.3°$.

The XRD analysis indicates the titanium oxide and calcium carbonate content of bauxite ore, in the form of anatase (TiO_2) and calcite ($CaCO_3$), respectively.

Calcination and Direct Reduction

Bauxite samples of 100 g weight were placed in a steel retort and were heated and subsequently reduced in a thermogravimetric (TGA) furnace. The sample was placed on top of a steel grid to ensure an even distribution of the upward moving gas between the ore particles. The sample temperature was measured in the middle of the bed and weight changes were recorded at regular intervals during the test. The gas inlet was at the top of the crucible, from which the gas moves through the hollow crucible wall before entering the sample at the bottom. Two thermocouples were used: one located in the furnace wall and the other located in the middle of the sample. The heating rate and target temperature were controlled based on the thermocouple readings in the furnace wall. Figure 4 shows a schematic of the TGA furnace used in this study.

The experimental target temperatures were 560, 660, 760, 860, 960, and 1060 °C with a deviation of ± 5 °C. The heating was performed in a 0.25 Nl/min argon stream from room temperature to the target temperature with a heating rate of 10 °C /min. Then 0.25 Nl/min of H_2 gas flow was introduced for 2 h reduction. The cooling after the reduction was done under Ar flow for 1 h.

The reduced bauxite samples were analyzed by XRD for phase analysis in a 10 to 75° wavelength and 0.02° step size. However, the microstructure was studied using JXA-8500F™ Electron Probe Micro-Analyzer (EPMA) with 15 kV voltage.

Results

Thermogravimetric Results

In Fig. 5, the thermogravimetric results for the calcination step are presented. The starting point in Fig. 5 is defined when the samples reached 300 °C, to minimize the buoyancy effect at lower temperatures in the mass losses. This effect becomes negligible when the temperature increases. The ending point is defined when the samples reached the target temperature and before the introduction of H_2 in the furnace bed.

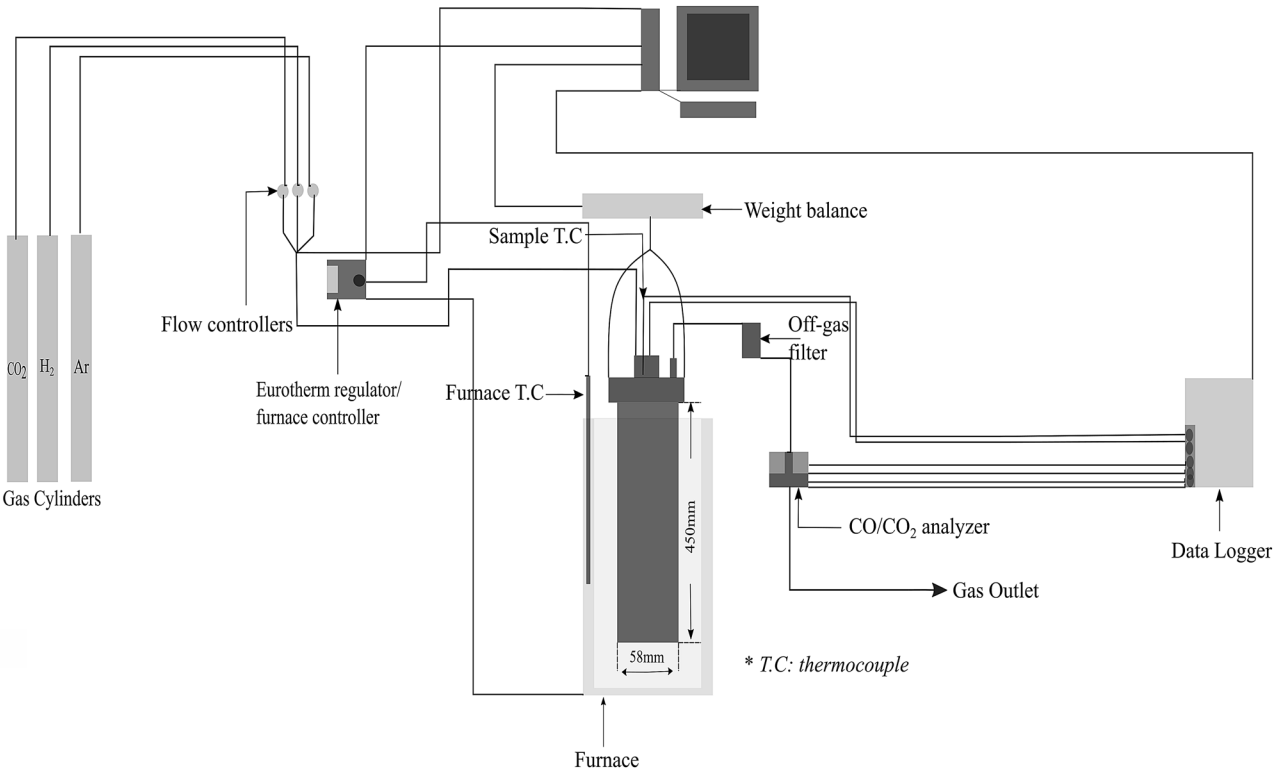

Fig. 4 Schematic of the thermogravimetric furnace setup. The crucible is hanging in a scale, recording the weight changes and the data from weight balance, and the gas analysis ends up to the data logger

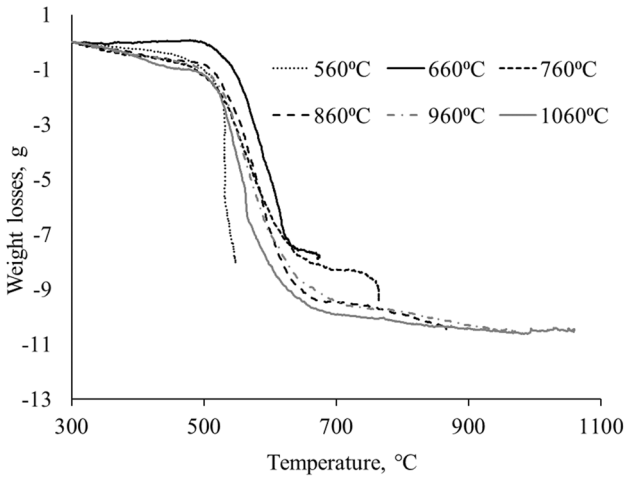

Fig. 5 Thermogravimetric results in the calcination step

The results in Fig. 5 indicate that the calcination step was not completed for the samples treated at 560, 660 °C, and 760 °C. While for the samples treated at 860, 960, and 1060 °C, it seems that the calcination completed since no further weigh losses occurred. For this reason, the reduction step was studied for the higher temperatures only.

According to the above results, the calcination is partially completed for the temperatures 560, 660, and 760 °C and thus the results are not considered suitable to provide a clear image of the kinetics of reduction at these temperatures. This is because the kinetics of reduction at these temperatures is affected due to the simultaneous calcination and reduction phenomena that have inevitable effect on the kinetic curves. However, the kinetic study focused on the samples treated at 860, 960, and 1060 °C, where the calcination is almost complete before the H_2 flow step.

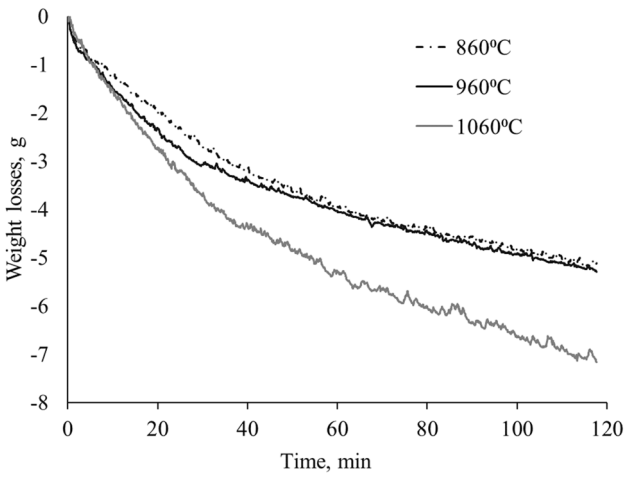

Fig. 6 Weight losses plotted against time in the reduction step for the samples treated at 860, 960, and 1060 °C

Figure 6 presents the weight losses for the samples treated at 860, 960, and 1060 °C in the reduction step. The weight losses normalized when H_2 introduces the sample bed. For the reduction step, the gas changes from Ar to Ar and H_2 mixture, even if the total flow rate is constant and this should minimize the effect of the change in the gas: the effect of hydrogen in the weight losses has been taken into consideration for normalizing the weigh losses. The effect of hydrogen was calculated to be 0.67 g. It is obvious that for the sample treated at 1060 °C, the weight losses were higher, due to the higher reduction temperature. The curves of the normalized weigh losses plotted against time of reduction indicate that the time was not enough to completely reduce the iron oxides from the samples by applying the studied conditions since no plateau in the curves was observed.

Phases Analysis of Reduced Bauxite

The mineralogical phases in the ore are changing during the heating and reduction of bauxite. Figure 7 shows the XRD results of the produced samples and it indicates that the phases existing in the bauxite ore have significantly changed after the calcination and reduction at different temperatures.

When the samples are heated and reduced at 560 and 660 °C, diaspore and boehmite have been completely transformed to aluminum oxide, Al_2O_3. Moreover, the peaks of hematite (Fe_2O_3) have disappeared and the peaks of magnetite (Fe_3O_4) and metallic iron (Fe) become the main Fe phases.

At 760 °C, Al_2O_3 is the only Al-containing phase. Metallic iron was detected with a characteristic peak at $2\theta = 44.7°$

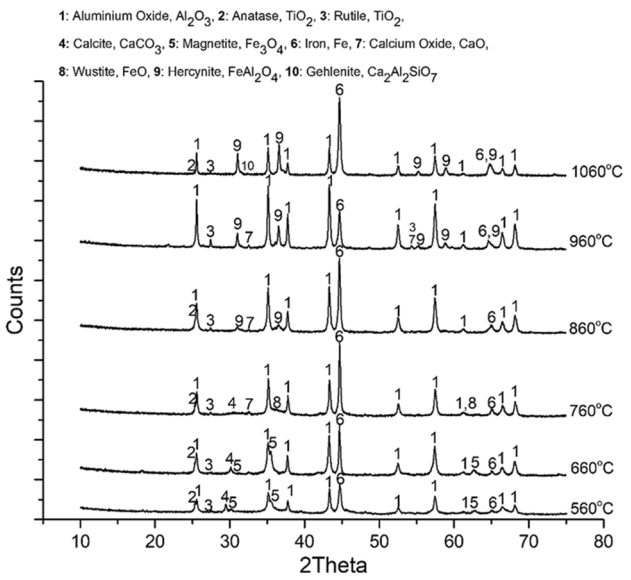

Fig. 7 XRD patterns of the samples obtained after the reduction at different temperatures

[3] and some small in intensity peaks of wustite (FeO) at around $2\theta = 36.2$ and 61.5°, and the second peak is overlapping with the peak of Al_2O_3. Titanium appears as anatase and rutile (TiO_2) for the samples treated up to 760 °C. The peaks of calcite have been detected for all of the temperatures up to 760 °C with the main peak at $2\theta = 29.7°$. At 760 °C, a small peak of calcium oxide appears at around $2\theta = 32.4$ and 54°.

At 860 °C, aluminum oxide and metallic iron are observed as we saw for lower temperatures and titanium appears as rutile and anatase. However, a spinel phase that is characterized as hercynite ($FeAl_2O_4$) has appeared in XRD spectrums, with main characteristic peaks at $2\theta = 31$ and 36.57° [16, 17]. At 960 °C and 1060 °C, the peaks of hercynite ($FeAl_2O_4$) become more intense in comparison with the pattern at 860 °C. Aluminum oxide and metallic iron are observed in the above patterns as in the lower temperatures. Titanium appears as rutile for the sample treated at 960 °C, while for the sample reduced at 1060 °C titanium is detected as anatase and rutile but with lower intensity peaks, in comparison with the sample treated at 960 °C which are difficult to observe in the diagram obtained.

For all the samples up to 960 °C, the peaks of SiO_2 have low intensity and, due to the detection limits in XRD analysis, are not clearly visible in the patterns. Calcium appears as calcium oxide for the samples treated at 860 °C and 960 °C. At 1060 °C, we could not detect any SiO_2 and CaO peaks but instead a low intensity peak of gehlenite ($2CaO{\cdot}Al_2O_3{\cdot}SiO_2$) is detected at $2\theta = 31.4°$.

Microstructural Analysis

The microprobe images for the reduced samples at 560, 760, and 1060 °C are shown in Fig. 8, at × 40 magnification. The sample reduced at 560 °C (Fig. 8a) is rich in aluminum oxide. Iron is distributed in two main areas: one is high in Fe with no oxygen, while the other one contains both Fe and oxygen. SiO_2 is distributed mostly in the area with rich Fe; however, the XRD analysis does not detect any compound that contains both Fe and Si.

The X-ray mapping of the reduced sample at 760 °C, shown in Fig. 8b, indicates locations rich in Fe with no or very weak oxygen intensities, confirming the presence of metallic iron and wustite. The high alumina content is also observed for this sample, while the low silica and titanium oxide content is obvious from the distribution observed for the sample reduced at 560 °C. In addition, there are small particles with high calcium content, which are most likely calcite ($CaCO_3$) based on the existence of small amount of calcite in the sample, Fig. 7.

For the sample reduced at 1060 °C, a similar microstructure is observed for the Al, Si, and Ti oxides in the reduced samples at lower temperatures. However, in the area rich in Fe there is no oxygen content, showing higher reduction to metallic iron. However, in the metallic iron particle it seems that there are areas rich in alumina oxide, surrounded by metallic iron after the reduction. Moreover, some of the alumina particles having a circular shape (* in Fig. 8c) seem that they contain also low concentrations of iron and oxygen.

Discussion

Calcination Reactions and Kinetics

According to the XRD results in Fig. 7, the transformation of diaspore and boehmite to Al_2O_3 (reaction (5)) occurs at temperatures lower than 560 °C, as indicated, and the decomposition completed at 560 °C [15] where Al_2O_3 was the only Al phase. The theoretical calculations seem to be in close agreement with the experimental observations.

No further observation of goethite at higher temperatures, according to XRD and EPMA results, confirms that its decomposition has been completed, which is furthermore expected based on the Gibbs energy changes of reaction (6) shown in Fig. 2.

In order to understand better the phenomena during calcination at different temperatures, the fraction conversion by calcination can be calculated.

The decomposition of diaspore, boehmite, goethite and also the decomposition of $CaCO_3$ are the main reasons for the weight losses during heating in Ar. Thus, the fraction conversion for the weight changes during heating can be calculated according to the following Eq. (8).

$$X_{\text{calcination}} = \frac{\Delta W}{W_{\text{in}} \times \left(\frac{\text{LoI}}{100}\right)}, \tag{8}$$

where ΔW is the change in the mass of the sample as recorder during the experiment, W_{in} is the initial mass of the sample and LoI is the loss of ignition (Table 1), which corresponds to the expected weight losses during heating.

The calculated $X_{\text{calcination}}$ values are given in the following diagram, Fig. 9. Calculating the theoretical weight losses for diaspore and calcite, according to the following Eqs. (9) and (10), the dehydration and decomposition seem to contribute mostly in the total weigh changes, Eq. (11).

$$X_{\text{dehydration}} = \frac{W_{H_2O}}{\Delta W_{\text{total}}} \tag{9}$$

$$X_{\text{decomposition}} = \frac{W_{CO_2}}{\Delta W_{\text{total}}} \tag{10}$$

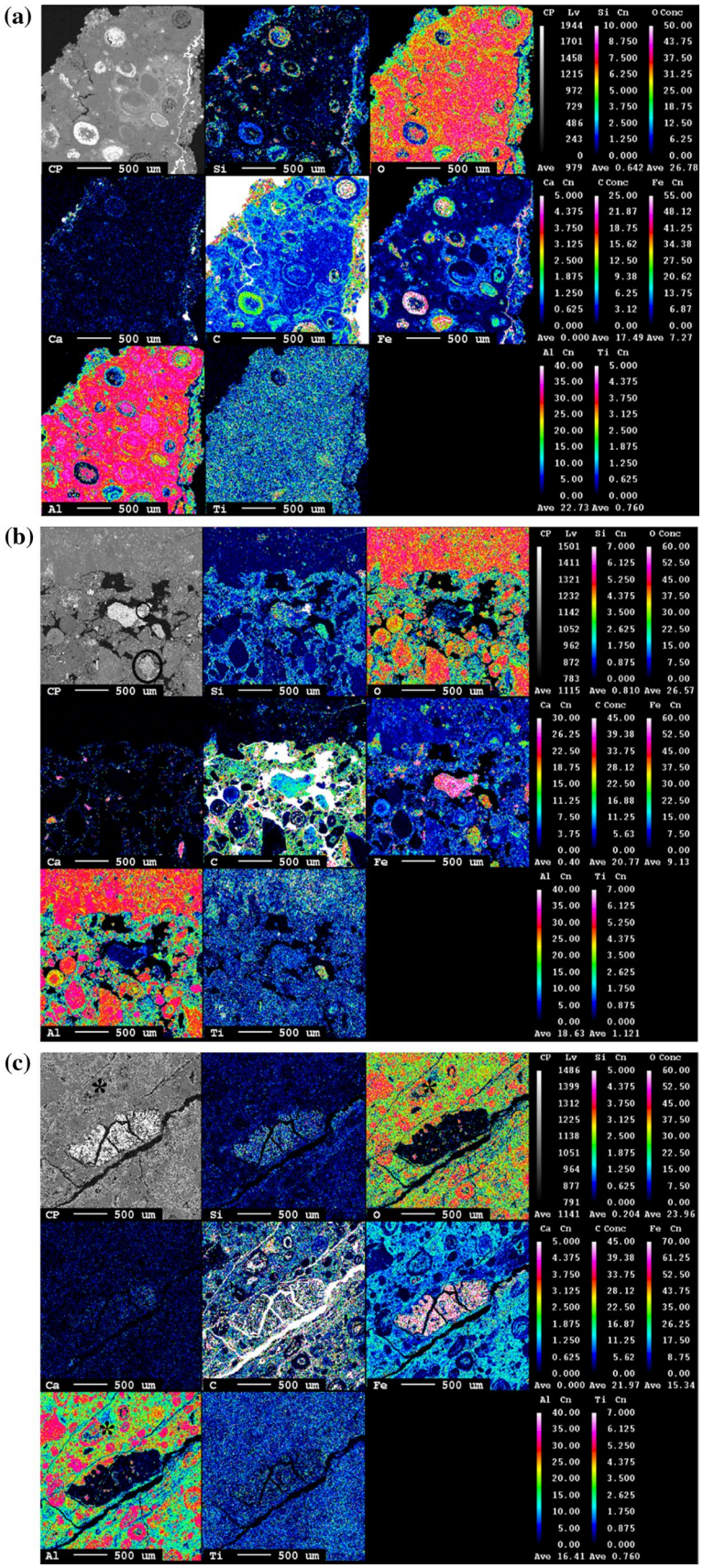

Fig. 8 EPMA analysis of the samples reduced at **a** 560 °C, **b** 760 °C, and **c** 1060 °C, in × 40 magnification. The spherical area in image b represents the coexistence of Fe with oxygen and the matrix *In image c, the aluminum oxide containing iron fine particles. (Color figure online)

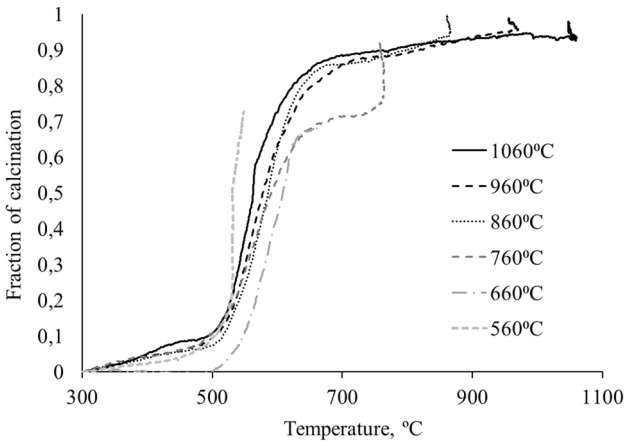

Fig. 9 Fraction of calcination at the different examined temperatures

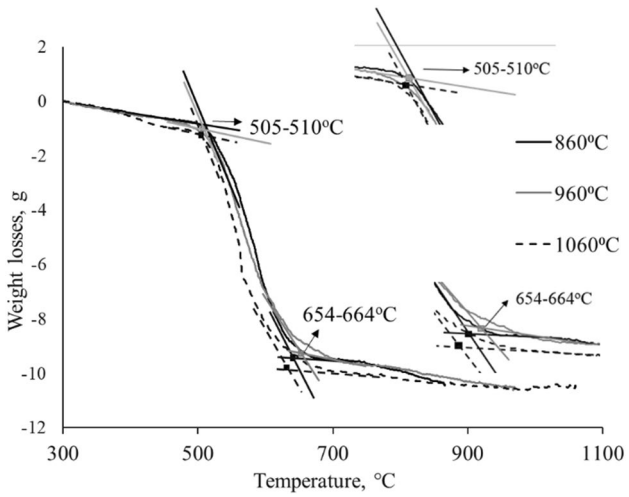

Fig. 10 The onset temperatures for diaspore and calcite decomposition for the samples treated to higher temperatures

$$X_{\text{dehydration}} + X_{\text{decomposition}} = 0.92, \tag{11}$$

where W_{H_2O} and W_{CO_2} correspond to the losses of H_2O and CO_2 of diaspore and calcite, respectively, according to reaction (5) and (7), during heating. ΔW_{total} is the theoretical total mass losses during heating (LoI).

Obviously, the calcination seems to be completed for the temperatures 860, 960, and 1060 °C.

The dehydration of diaspore starts at temperatures higher than 300 °C, while the decomposition of calcite starts at higher temperatures. According to the literature, diaspore is transformed to alumina oxide when heated to 500 °C [18], while the decomposition of calcite is completed at temperature higher than 750 °C [19]. During heating to temperatures of 560, 660, 760 °C, the calcination of calcite is slow and most likely is not completed during the heating step, which is confirmed by the XRD analysis. According to I. Halikia et al., the decomposition of calcite occurs between 635 and 865 °C [20]. Figure 9 confirms furthermore the above observations.

In order to estimate the starting and ending temperatures for diaspore and calcite decomposition, the cross point of the drawn tangents method was studied, Fig. 10. The CO_2 gas concentration in the gas outlet (leaving the sample bed) during heating at temperatures higher than 860 °C was studied for the calcite decomposition, Fig. 11.

According to the presented data in Fig. 10, the main temperature for the diaspore decomposition is in the range of 505 to 510 °C, as done in the same heating regime for all of the presented samples. For calcite, it seems that the decomposition starts in the range of 654 to 664 °C, as determined through the cross point of the drawn tangents on the weight losses. This starting temperature range is lower than the theoretical temperature. This may be due to the low CO_2 pressure in the gas mixture and providing conditions for calcite decomposition from lower temperatures.

In Fig. 11, the CO_2 gas leaving the sample bed was studied to investigate the decomposition of calcite. The highest decomposition rate of calcite is above 760 °C based on the CO_2 gas analysis and the decomposition seems to be completed above 850 °C, Fig. 11, as we also see in the XRD analysis where calcite and calcium oxide co-exist at the sample treated at 760 °C. This indicated that the decomposition needs higher temperature to be completed. Finally, the onset temperature for the decomposition of diaspore can be determined from the mass loss changes as outline above and schematically shown in Fig. 10. The approximate temperature for diaspore decomposition is estimated to be at the range of 505–510 °C after applying a heating rate of 10 °C/min, which is in agreement with the literature [3, 15]. However, these temperatures are higher than the theoretical dissociation temperature of 300 °C. Thus, we may claim that the decomposition of diaspore is controlled kinetically.

Kinetics of Iron Oxide Reduction

The reduction of hematite to magnetite by hydrogen gas starts at low temperatures. Thermodynamically, chemical reaction (1) can occur at even room temperature; however, from a kinetic point of view it needs higher temperatures. Therefore, we see that within two hours of reduction at 560 °C and 660 °C reaction (1) is not completed, while the extend of reduction is higher at higher temperatures.

Moreover, for the reduced sample at 560 °C the two phases of magnetite and iron co-exist as both XRD and EPMA analyses confirm. At 760 °C, metallic iron and wustite were the detected phase of iron by the XRD analysis, which is further confirmed by the EPMA analysis. The reduction by H_2 at 860 °C and higher temperatures causes

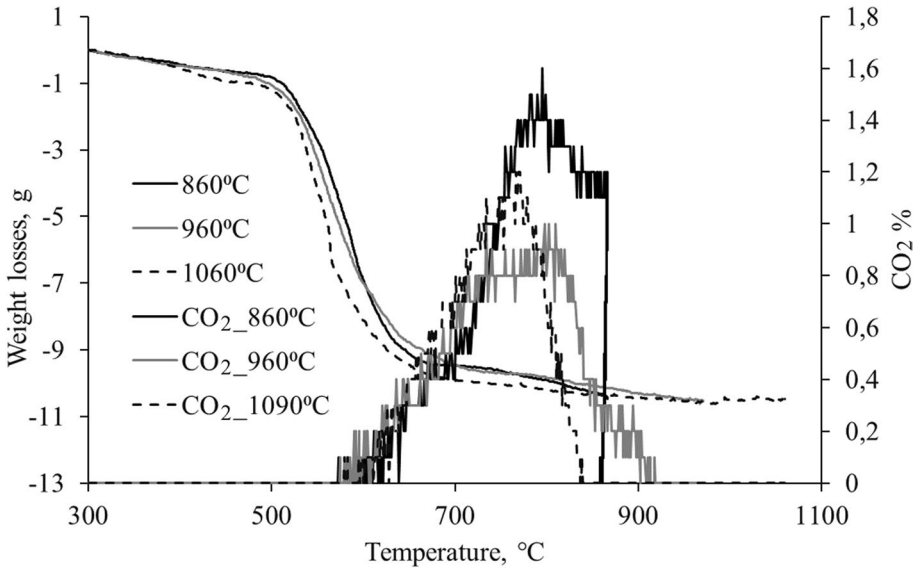

Fig. 11 The weigh losses in the calcination step and the CO_2 release from the samples during heating to higher temperatures

hercynite ($FeAl_2O_4$) formation according to XRD results. At 1060 °C, both EPMA and XRD analyses confirm the reduction to metallic iron. According to EPMA analysis, the metallic iron phase has 'cracks' as expected due to the higher reduction temperature. Furthermore, in some of the aluminum oxide particles, low concentrations of iron oxide are also detected, (Fig. 8c). Thus, we may say that those particles represent the phase called hercynite.

Zhuo et al. suggested a mechanism for the formation of hercynite [21] in which they claim that it is possible that the Fe_3O_4 and FeO are formed during reduction and they react with Fe and Al_2O_3 through reactions (12) and (14) to form hercynite [21]. Moreover, according to Maniatis et al. [22] if the atmosphere is reducing, iron is reduced to divalent form and the initially existing oxides are dissociated. The resulting ferrous iron is partly dissolved into the matrix and partly forms hercynite [22]. According to [23, 24], the formation of wustite is the reason for the hercynite formation in the presence of alumina in the samples. The formation of the above phase seems to retard the complete reduction of iron oxides [24, 25].

$$Fe_3O_4 + 4Al_2O_3 + Fe = 4FeAl_2O_4 \quad (12)$$

$$FeO + Al_2O_3 = FeAl_2O_4 \quad (13)$$

$$Fe_3O_4 + 3Al_2O_3 + H_2 = 3FeAl_2O_4 + H_2O. \quad (14)$$

According to [21], it is possible that at 900 °C part of hercynite continues to be reduced to metallic iron and alumina oxide, and at temperature higher than 1000 °C hercynite can be completely reduced using H_2 gas. According to the theoretical calculations, the reduction of hercynite requires temperatures higher than 2100 °C to occur under 1 atm pressure, which is the standard condition and equal molar ratio of H_2/H_2O in the gas. However, when the molar ratio of H_2/H_2O is significantly higher, which is due to the continuous hydrogen supply over the sample bed, the hercynite reduction is possible as shown by the changes of the Gibbs energy of reaction (15) for higher reducing gas mixtures (higher PH_2/PH_2O ratios) in Fig. 12. For instance, the reduction of hercynite can take place at temperatures higher than 1273 K by the gas mixtures with H_2/H_2O ratios above 100. In practice, it means that the sample must be under hydrogen flow so that the amount of H_2O that is released becomes low enough that the gas mixture in the bed reaches the conditions for the hercynite reduction. As T. Lu et al. have observed, temperatures greater than 1000 °C are required for the reduction of hercynite using carbon and carbon monoxide as reductants [26]. Observing no hercynite reduction from our sample for temperatures higher than 960 °C may be due to not enough time at this temperature after its formation, if we assume that the H_2/H_2O ratio is large enough for its reduction at the latest minutes of the reduction step.

$$FeAl_2O_4 + H_{2(g)} = Fe + Al_2O_3 + H_2O_{(g)}. \quad (15)$$

The small amount of wustite detected at the sample treated at 760 °C, Fig. 7 can be in agreement with the above theories and explain the appearance of hercynite in the higher temperatures but the mechanism for the formation of hercynite and its reduction is not clear yet and is of interest in our further studies before a possible mechanism can be suggested.

To understand the reduction kinetics, the rate and extend of reduction can be calculated from the fraction of conversion, given by Eq. (16)

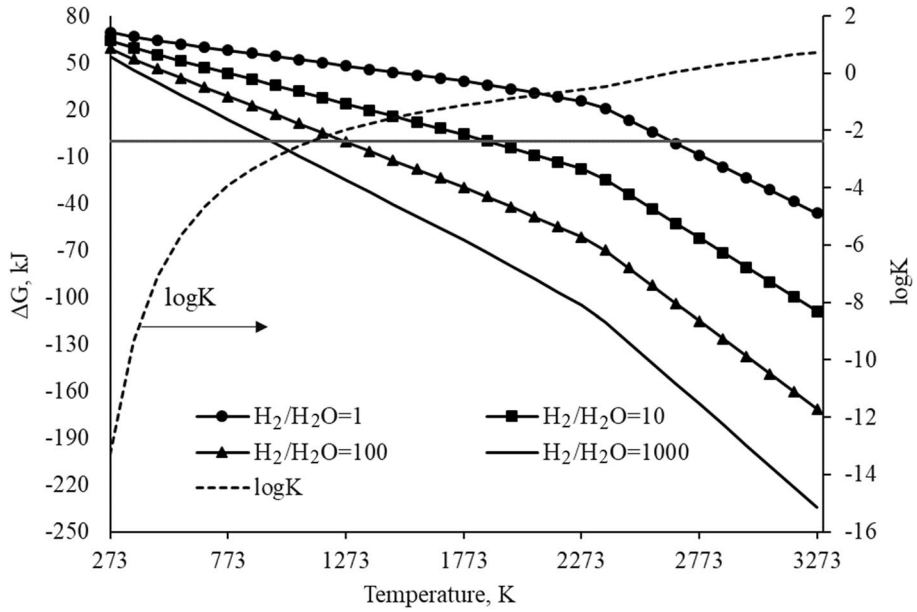

Fig. 12 Changes in the Gibbs energy for reaction (15) against temperature for different H_2/H_2O ratios, and changes in log *K* with increasing temperature at standard conditions as calculated using HSC software version 7.1 for pure compounds

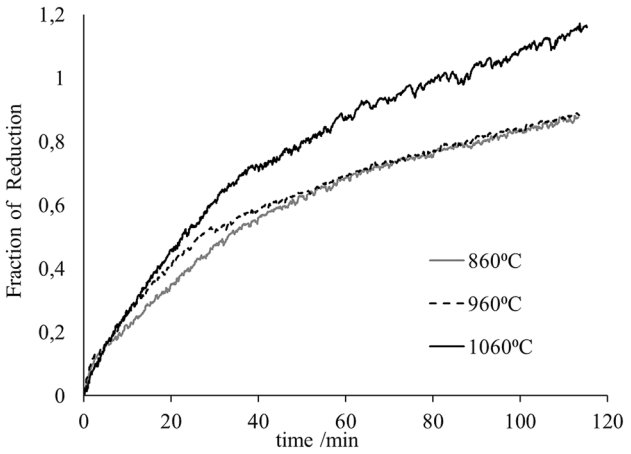

Fig. 13 Fraction of reduction vs time for the tests at higher temperatures

$$X_{\text{red}} = \frac{\Delta W_{\text{red}}}{W_{\text{in}} \times \left(\frac{(\text{wt\% of oxygen in hematite})}{100} \right)}, \tag{16}$$

where ΔW_{red} corresponds to the weight losses during reduction as measured during the experiments, W_{in} is the input mass of the sample and wt% *of* O_2 *in hematite* is the oxygen content of hematite contained in the bauxite ore. The calculated X_{red}-values during the reduction are shown in Fig. 13.

Figure 13 shows that the rate and extend of reduction is higher for the sample reduced at 1060 °C than at 860 and 960 °C, as expected based on the observation in Fig. 6. The rate of reduction is faster for higher reduction temperatures. The reduction to metallic iron seems to increase with increasing the temperature; however, the formation of hercynite seems to retard the complete reduction to metallic iron [24] according to XRD and EPMA results and the literature. The fraction of conversion seems to be more than 1 for the sample treated at 1060 °C and this is possible due to some inhomogeneities among the samples used and thus the slightly higher iron content than the one measured in the bauxite sample. As an example, if the iron content is 19% after calcination, the α is equal to 1.16 but if iron content is 22%, then the α is equal to 1.04 and α is even closer to 1 when iron content is 23%. This means that even a 1% difference in the iron content can create up to 10% differences in the fraction of conversion values and more experimental work is required to define the exact effect of the uncertainties. Furthermore, as we mentioned previously, the broad range of particle size 5–25 mm affects the efficiency of the reduction step and this is obvious in the X_{red} curves at Fig. 13. The fraction of reduction for the sample treated at 860 °C seems to be almost the same as the sample treated at 960 °C, which means that the Fe_2O_3/Al_2O_3 ratio is higher in the sample treated at 860 °C and this is due to some inhomogeneities within and among the ore particles. As mentioned in a previous section, the possible errors in the mass readings due to the gas changes have been taken into consideration to minimize this effect, so according to the above observations we may claim that the inhomogeneities along the particles should be the key source of uncertainty in this case.

Conclusions

Calcination and reduction of bauxite ore by hydrogen was studied by thermogravimetry method supported by microstructural and phase analysis. The main conclusions of this preliminary work are summarized as follows:

- The dehydration of diaspore and boehmite occurs at 505–510 °C, under non-isothermal conditions.
- The decomposition of calcite in the ore commences at around 645 °C and is faster at higher temperatures.
- The reduction of hematite to magnetite starts at temperatures below 560 °C with slow rate.
- The reduction of magnetite to metallic iron occurs at above 560 °C and is faster at higher temperatures.
- At higher temperatures, i.e., 860, 960, and 1060 °C, the formation of hercynite ($FeAl_2O_4$) retards the complete reduction to metallic iron.

Acknowledgements Open Access funding provided by NTNU Norwegian University of Science and Technology (incl St. Olavs Hospital - Trondheim University Hospital). The research leading to these results has been performed within the ENSUREAL project and received funding from the European Community's Horizon 2020 Program (H2020/2014-2020) under Grant agreement No 767533. We thank the support from Irene Bragstad at SINTEF for her great assistance in the implementation of the experiments.

References

1. Kloprogge JT et al (2002) Thermal decomposition of bauxite minerals: infrared emission spectroscopy of gibbsite, boehmite and diaspore. J Mater Sci 37(6):1121–1129. https://doi.org/10.1023/a:1014303119055
2. Tam P et al (2017) Carbothermic reduction of bauxite residue for iron recovery and subsequent aluminium recovery from slag leaching, Travaux 46, In: Proceedings of 35th international ICSOBA conference, Hamburg, Germany, 2–5 Oct 2017. https://doi.org/10.5281/zenodo.1040789
3. Samouhos M et al (2016) Kinetic study of non-isothermal decomposition of a composite diasporic-boehmitic bauxite. IOP Conf Ser 123:012048. https://doi.org/10.1088/1757-899x/123/1/012048
4. de Aquino TF et al (2011) Mineralogical and physical-chemical characterization of a bauxite ore from Lages, Santa Catarina, Brazil, for refractory production. Miner Process Extr Metall Rev 32(3):137–149. https://doi.org/10.1080/08827508.2010.531069
5. Bonomi C et al (2018) Scandium and titanium recovery from bauxite residue by direct leaching with a brønsted acidic ionic liquid. Metals. https://doi.org/10.3390/met8100834
6. Lazou A, Van der Eijk C, Balomenos E, Safarian J (2019) Smelting reduction of bauxite residue and beneficiation by-product in view of a leachable slag and pig iron production. In: Proceedings of European metallurgical conference, Düsseldorf, Germany, pp 17–34
7. Safarian J (2018) Extraction of iron and ferrosilicon alloy from low-grade bauxite ores. In: Davis B, et al. (eds) Extraction 2018 the minerals, metals & materials series. Springer, Cham. https://doi.org/10.1007/978-3-319-95022-8_66
8. Vafeias M et al (2018) From red to grey: revisiting the Pedersen process to achieve holistic bauxite ore utilisation. In: Proceedings of the 2nd international bauxite residue valorisation and best practices conference, Athens, Greece, 7–10 May 2018, pp 111–117
9. Safarian J, Kolbeinsen L (2016) Sustainability in alumina production from bauxite. In: Kongoli F, Kumar P, Senchenko A, Klein B, Silva AC, Sun C, Mingan W (eds) Sustainable Industrial Processing Summit SIPS 2016 volume 5: starkey international symposium/mineral processing. Montreal, FLOGEN Star Outreach, pp 75–82
10. Azof FI et al (2018) Characteristics of calcium-aluminate slags and pig iron produced from smelting-reduction of low-grade bauxites. Metall Mater Trans B 49(5):2400–2420. https://doi.org/10.1007/s11663-018-1353-1
11. Wagner D et al (2006) A laboratory study of the reduction of iron oxides by hydrogen. TMS Fall Extraction & Processing Meeting: Sohn Int'l Symposium, San Diego, pp 111–120
12. Nyankson E, Kolbeinsen L (2015) Kinetics of direct iron ore reduction with CO-H_2 gas mixtures. Int J Eng Res Technol. https://doi.org/10.17577/IJERTV4IS040955
13. Longbottom R, Kolbeinsen L (2008) Iron ore reduction with CO and H_2 gas mixtures—thermodynamic and kinetic modelling. In: Proceedings of the 4th Ulcos seminar – New Direct Reduction (DR), 1 & 2 October 2008, pp 1–13
14. Jozwiak WK et al (2007) Reduction behavior of iron oxides in hydrogen and carbon monoxide atmospheres. Appl Catal A 326:17–27. https://doi.org/10.1016/j.apcata.2007.03.021
15. Angelopoulos P et al (2016) Thermal decomposition kinetics of greek diasporic bauxite. In: Proceedings of OPMR2016 – Opportunities in Processing of Metal Resources in South East Europe, Budapest, 28–30 November 2016, pp 191–200
16. Hertel T et al (2016) A proposal for a 100 % use of bauxite residue towards inorganic polymer mortar. J Sustain Metall 2(4):394–404. https://doi.org/10.1007/s40831-016-0080-6
17. Samouhos M et al (2013) Greek "red mud" residue: a study of microwave reductive roasting followed by magnetic separation for a metallic iron recovery process. J Hazard Mater 254–255:193–205. https://doi.org/10.1016/j.jhazmat.2013.03.059
18. Yang Hua-ming Hu, Yue-hua Y-G, Wei-qin Ao, Guan-zhou Q (2004) Alteration of diaspore by thermal treatment. J Cent South Univ Technol 11(2):173–175. https://doi.org/10.1007/s11771-004-0036-z
19. Pehlivan A et al (2012) Alumina extraction from low-grade diasporic bauxite By pyro-hydro metallurgical process. Sak Univ J Sci. https://doi.org/10.5505/saufbe.2012.73645
20. Halikia I, Zoumpoulakis L, Christodoulou E, Prattis D (2011) Kinetic study of the thermal decomposition of calcium carbonate by isothermal methods of analysis. Eur J Miner Process Environ Prot 1(2):89–102
21. Zhou L et al (2016) Catalytic methane decomposition over Fe-Al_2O_3. ChemSusChem 9(11):1243–1248. https://doi.org/10.1002/cssc.201600310

22. Maniatis Y et al (2006) Effect of reducing atmosphere on minerals and iron oxides developed in fired clays: the role of Ca. J Am Ceram Soc 66(11):773–781. https://doi.org/10.1111/j.1151-2916.1983.tb10561.x
23. Pickles CA et al (2012) A study of reduction and magnetic separation of iron from high iron bauxite ore. Can Metall Q 51(4):424–433. https://doi.org/10.1179/1879139512Y.0000000038
24. Zhou X et al (2018) Enhancing the reduction of high-aluminium iron ore by synergistic reducing with high-manganese iron ore. Metals. https://doi.org/10.3390/met9010015
25. Dankwah JR, Fosu AY, Fosu N, Koshy P (2015) Carbothermal upgrading of the awaso bauxite ore using waste pure water sachets as reductant. Ghana Min J 16(2):58–64. https://doi.org/10.4314/gm.v16i2.8
26. Lu T et al (2012) Carbothermal reductive upgrading of a bauxite ore using microwave radiation. High Temp Mater Process 31:139–148. https://doi.org/10.1515/htmp-2012-0002